



ISSN: 0067-2904

Fusion Images Techniques for Motion Pixel in A blurred Image

Nawras badeaa mohammed¹, Haidar J. Mohamad^{1*}, Heba Kh. Abbas²

¹ Department of Physics, College of Science, Mustansiriyah University, Baghdad, Iraq

² Department of Physics, College of Science for Women, University of Baghdad, Baghdad, Iraq

Received: 1/4/2023

Accepted: 29/5/2023

Published: 30/6/2024

Abstract

Fusing digital images is an essential step in digital image processing, as it allows for integrating information from two or more images into a single image of high quality and clarity. This work fused images resulting from motion blur (left and right) with blur block sizes of 3, 5, 7, 9, and 11. The image resulting from the blur towards the right was combined with the image resulting from the blur towards the left for the same degree of blur using traditional techniques such as addition, multiplication, and new suggested techniques, namely absolute real standard deviation, binary standard deviation, real Covariance, and binary Covariance. The data examined by quality assessment methods with the reference depends on Mutual Information, Correlation Coefficient, Structural Similarity Index metric, Structural Content, Normalized Cross Correlation, and without references like Blind Reference, less Spatial Image Quality Evaluator, Naturalness Image Quality Evaluator, Perception-based Image Quality Evaluator, and Entropy. The best combination method was binary covariance and standard binary division.

Keyword: motion blur, mathematical fusion, real and binary standard deviation, real and binary CV.

تقنيات دمج الصور لوحدات البيكسل المتحركة في صورة ضبابية

نورس بديع محمد¹، حيدر جواد محمد^{1*}، هبة خضير عباس²

¹ قسم الفيزياء، كلية العلوم، الجامعة المستنصرية، بغداد، العراق

² قسم الفيزياء، كلية العلوم للبنات، جامعة بغداد، بغداد، العراق

الخلاصة

يعد اندماج الصور الرقمية خطوة أساسية في معالجة الصور الرقمية، حيث يسمح بدمج المعلومات من صورتين أو أكثر في صورة واحدة عالية الجودة والوضوح. دمج هذا العمل الصور الناتجة عن ضبابية الحركة (يمين ويسار) مع كتلة ضبابية بحجم 3 و 5 و 7 و 9 و 11. الصورة الناتجة عن التمويه باتجاه اليمين تم دمجها مع الصورة الناتجة عن التمويه باتجاه اليسار لنفس الدرجة من التمويه باستخدام التقنيات التقليدية مثل الجمع والضرب والتقنيات المقترحة الجديدة وهي الانحراف المعياري المطلق والانحراف المعياري الثنائي والتغاير الحقيقي والتغاير الثنائي. البيانات التي تم فحصها بواسطة طرق تقييم الجودة مع الصورة الأصلية والتي تعتمد على المعلومات المتبادلة، ومعامل الارتباط، ومقياس مؤشر التشابه الهيكلي، والمحتوى الهيكلي، والارتباط المعياري المتقاطع وبدون مرجع مثل مرجع أقل مقيم جودة الصورة المكانية، مقيم جودة الصورة الطبيعية،

*Email: haidar.mohamad@uomustansiriyah.edu.iq

الصورة القائمة على الإدراك مقيّم الجودة، إنتروبيا. كانت أفضل طريقة للدمج هي طريقة التباير الثاني والانحراف المعياري الثاني

1. Introduction

Image fusion combines data from two or more images and obtains a single, more comprehensive image using a specialized application. This application studies the features of multiple images within the same scene, utilizing redundant and complementary information among the image data [1]. Employing specific algorithms to extract relevant feature data from multiple images [2] can create a new image with more comprehensive and precise details through image fusion technology [3]. Depending on the input image's kinds, image fusion can be divided into various categories: remote sensing, medical and military imaging [4], astronomy, multi-imaging focusing, multiple exposures, infrared and visual image fusion [5], and more. Image-merging technology has been advancing for more than four decades, with increasing research techniques and applications emerging [6]. This technology offers a range of advantages, such as image sharpening [7], optimizing features [8], classifying [9], and creating stereoscopic datasets [10]. Multi-sensor image fusion also provides benefits in terms of operational scale, spatial-temporal characteristics, system performance, reduced ambiguity, and improved reliability. It can be divided into different categories: pixel level, feature level, symbol level, and area-based fusion. The highest level of technology is block-level, which is a multi-stage representation and measurements by regions [11].

Recent studies explored image-merging technology, such as Berhan Oume Adame *et al.* (2020) [12], who produced a comprehensive survey and comparative analysis of existing medical image fusion algorithms. Many image-merging kinds of literature can be categorized into five distinct methods: morphological methods, human value system operator-based methods, subscale decomposition methods, neural network-based methods, and methods based on fuzzy logic. Each method offers unique advantages and can be used to achieve different results. This research concludes that integrating medical images in various combinations can benefit medical diagnosis and examination. Recent advances in deep learning, artificial intelligence, and optimization technologies have enabled the development of more efficient image-merging algorithms.

A two-scale multimodal medical image merging algorithm was suggested by Xin Qi *et al.* (2022) [13] based on structure preservation. This algorithm decomposes the source images into two scales, taking advantage of the multi-scale information of the images. Additionally, the algorithm utilizes the structure preservation characteristic of the iterative joint bilateral filter and applies Convolution Neural Network (CNN) in medical image fusion. Contrast experiments showed that the suggested algorithm has higher efficiency than competing algorithms, although its computational speed is not ideal.

Yifan Xiao *et al.* (2022) [14] described four types of multi-focus image fusion techniques: a transform domain method, a boundary segmentation method, a deep learning method, and a combinatorial fusion method. The methods were thoroughly classified, and their benefits and drawbacks were compared and evaluated. Depending on the scenario, it is essential to choose the suitable method. Furthermore, the frequently used evaluation indicators are stated, allowing for an objective evaluation that is more precise than the subjective evaluation while also taking less effort and time. After analyzing the shortcomings of current applications and methods, a solution has been proposed: multi-focus image fusion. This technique can successfully address the field problem in optical lens areas; however, further development is needed to improve its universality and increase its fusion space. To ensure the highest quality

of fusion, it is essential to prioritize the effective use of time, with the ultimate goal of achieving real-time fusion.

This study seeks to improve the clarity of distorted images' grey level (Lena, cameraman, and personal) utilizing image fusion techniques after distorting the input images using the linear motion blur method left and right. Traditional techniques, such as (addition and multiplicative) and statistical merging techniques based on weights (real standard deviation, binary standard deviation, real covariance, and binary covariance), were employed. The quality of the resulting images was evaluated using statistical criteria dependent on the reference (Mutual Information, Correlation Coefficient, Structural Similarity Index metric, Structural Content, and Normalized Cross Correlation) and without reference (Blind Reference less Image Spatial Quality Evaluator, Naturalness Image Quality Evaluator, Perception-based Image Quality Evaluator, and Entropy).

2. Theory and Methods

To improve the clarity of distorted images, researchers proposed image fusion techniques that involve distorting the input images using the motion blur method horizontally, left, and right, followed by traditional mathematical techniques such as tearing and beating or statistical merging techniques based on weights (standard deviation and covariance)[15]. The resulting image quality was then evaluated using statistical criteria with the presence and absence of the reference [16]. The recovery of such images relies heavily on estimating motion blur parameters. The general form of the motion blur function was given as follows [17,18]:

$$h(i, j) = \begin{cases} \frac{1}{L} & \text{if } \sqrt{i^2 + j^2} \leq \frac{L}{2} \text{ and } \frac{i}{j} = -\tan(\phi) \\ 0 & \text{otherwise} \end{cases} \quad (1)$$

Where L is motion length, and ϕ is motion direction, which are considered the two important parameters. The weighted factors are[9]:

$$\sigma_{I_{A,B}}(i, j) = \sqrt{\sum_{i=1}^m \sum_{j=1}^n (I(i, j) - \mu)^2} \quad (2)$$

$$P1 = \frac{\sigma_{I_A}(i, j)}{\sigma_{I_A}(i, j) + \sigma_{I_B}(i, j)} \quad (3)$$

$$P2 = (1 - P1) \quad (4)$$

Where $\sigma_{I_{A,B}}$ The standard deviation for refer image, μ , indicates that mean, P1, and P2 are the selected weight factor values, which is a critical aspect of the algorithm. These values can be set based on human experience or determined dynamically.

The proposed integration technique was also applied based on the statistical standard direct covariance (CV) image fusion. Covariance is a way of calculating the degree to which two random variables change together [19]. If the higher values of one measure mostly match the higher values of the other, and the same holds for the smaller values, i.e., the variables likely to behave similarly, covariance is a positive value. The covariance sign, therefore, shows the tendency in the linear relationship between the variables. Mathematically covariance between two variables A and B is given as[20]:

$$CV_{I_{A,B}}(i, j) = \frac{1}{i \times j} \sum_{i=1}^m \sum_{j=1}^n (I_A(i, j) - \bar{I}_A)(I_B(i, j) - \bar{I}_B) \quad (5)$$

2.1 Quantitative Analysis Criteria

Based on mathematical modeling, quantitative analysis measures the quality of the merged image by taking a set of predefined quality indices to evaluate the spectral and spatial

similarities between the merged image (C) and the input images (A and B). Quantitative analysis was adopted by two approaches with a reference image and without a reference image. When a reference image is available, the performance of the merged image is evaluated using Mutual Information (MI), Correlation Coefficient (CC) [21], Structural Similarity Index Metric (SSIM), Structural Content (SC), and Normalized Cross Correlation (NCC). If the reference image is not available, the performance of the merged image is evaluated using metrics such as Structural Blind Reference less Image Spatial Quality Evaluator (BRISQUE) [22], Naturalness Image Quality Evaluator (NIQE)[23], Perception-based Image Quality Evaluator (PIQE) [22] and Entropy.

2.1.1 Quantitative analysis with the reference image

Mutual Information combines source image information and quantity detail to make the final picture. Maximum Mutual Information indicates a successful application of the image fusion method. This is defined as follows:

$$MI_{AC} = \sum_{AC} P_{A,C(a,c)} \log \left[\frac{P_{AC(a,c)}}{P_{A(a)}P_{C(c)}} \right] \quad (6)$$

Where $P_{A(a)}$ and $P_{C(c)}$ is the probability of the input image (A) histogram and fused image (C). $P_{A,C(a,c)}$ indicates a joint histogram of input image A and the fused image C. Fusion performance is good if the mutual information value is high [24].

2.1.1.1 Correlation Coefficient (CC)

It is utilized to determine the similarity of spectral features from the reference (A or B) and the fused image. (C). The value of CC has to approach +1, which reveals that the reference and fused images were similar; if the value of CC is less than one, variation increases [21].

$$CC = \frac{2C_C}{C_A + C_C} \quad (7)$$

C_A and C_C represent the reference (A) and fused image (C) correlation coefficients.

2.1.1.2 Structural Similarity Index (SSIM)

It compares the local patterns of pixel intensities between the source and fused images. The range ranges from -1 to 1. The value 1 indicates that the reference and fused images are similar [25].

$$SSIM = \frac{(2\mu_A\mu_C + C1)(2\sigma_{AC} + C2)}{(\mu_A^2 + \mu_C^2 + C1)(\sigma_A^2 + \sigma_C^2 + C2)} \quad (8)$$

where μ_A and μ_C are the mean intensities, σ_A and σ_C are standard deviations, σ_{AC} is the covariance of A and C, and C1 and C2 are small constants for A and C, respectively.

2.1.1.3 Structural Content (SC)

The structural content quality metric is expressed as:

$$SC = \frac{\sum_{i=1}^m \sum_{j=1}^n (A_{ij})^2}{\sum_{i=1}^m \sum_{j=1}^n (C_{ij})^2} \quad (9)$$

A higher value of SC shows that the image has poor quality.

2.1.1.4 Normalized Cross Correlation (NCC)

It compares signals and images in signal and image processing. Moving one image over the other and calculating the correlation coefficient at each position was used to measure similarity, a correlation coefficient of 1 means the signals or images match effectively [26].

$$NCC = \sum_{i=1}^m \sum_{j=1}^n \frac{A_{ij} C_{ij}}{A_{ij}^2} \quad (10)$$

Where A is the reference image, and C is the fused image.

2.1.2 Quantitative analysis with no reference image

This type of quality assessment can be represented as:

2.1.2.1 Structural Blind/Referenceless Image Spatial Quality Evaluator (BRISQUE)

It anticipates the BRISQUE measure via a Support Vector Regression (SVR) model based on a database of images with related Differential Mean Opinion Score (DMOS) values. The database contains images with known distortion, such as compression artifacts, blurring, and noise, and it contains pristine versions of the distorted images. The image to be scored must have at least one of the distortions for which the model was trained, using MATLAB statement (brisque) [25].

2.1.2.2 Naturalness Image Quality Evaluator (NIQE)

Calculates the no-reference image quality score for input image using the Naturalness Image Quality Evaluator (NIQE). NIQE compares input image to a default model computed from images of natural scenes. A smaller score indicates better perceptual quality using MATLAB statement (NIQE) [27].

2.1.2.3 Perception-based Image Quality Evaluator (PIQE)

A Perception-based Image Quality Evaluator (PIQE) is a non-reference perception-based image quality evaluation method for real-world images. It calculates the image quality score using the mean subtraction contrast normalization coefficient. PIQE is an unsupervised method that does not require a learning model [28].

2.1.2.4 Entropy (En)

It was utilized to gauge the information content in a fused image; when the entropy of a merged picture is high, there is much information [29].

$$En = - \sum_{g=0}^L h(j) \log h(j) \quad (11)$$

Where L indicates the total number of grey levels, $h(j)$ indicates the probability density distribution of grey level j , and E indicates entropy.

2.2 Proposed Method

All algorithms were programmed using MATLAB software. First, a motion-blur algorithm is designed for all fusion algorithms. The *fspecial* function used to determine blur function as $PSF = fspecial('motion', ln1, theta)$. The $ln1$ represents the linear motion of block size (3, 5, 7, 9, and 11). At the same time, $theta$ specifies the angle of motion in degrees (zero value is fixed in this study). The algorithm has two directions blur, namely left and right blur. The right to left blur code is $J\text{ Right} (:1:c2, :) = I (:1:c2, :)$, and from left to right using $J\text{ Left} (:c2+1:c, :) = I (:c2+1:c, :)$, where $c2 = c/2$, which means the image column divided by two.

The fusion algorithms are divided into two groups. The first group is the mathematical methods. The second group is statistical methods.

I. Mathematical methods algorithms

The mathematical fusion algorithms include the addition and multiplication method.

- In this method, the fused image was created by calculating with the average of corresponding pixels from both input images.
$$\text{Image fuse addition} = I_{\text{Right}} / 2 + I_{\text{Left}} / 2.$$
- The Multiplication methods combines two data sets by multiplying the pixel of the first image with the pixel of the second image. Fuse equation can be written as:
$$\text{Image fuse multiplication} = \text{sqrt}(I_{\text{Right}}) * \text{Sqrt}(I_{\text{Left}}).$$

II. Statistical method algorithms

Two statistical methods were designed, each divided into two sub-methods. The first method was a standard deviation, divided into real and binary sub-methods. At the same time, the second method was covariance which is divided into real and binary sub-methods.

- **Real standard deviation method**
Statistical image fusion techniques come from the direct statistical techniques. This method assigns various weights to the related source images, which means that the pixels of gray value are multiplied by various factors as stated below:
$$\text{Proposed method P1} = \text{Standard deviation } I_{\text{Right}} / (\text{Standard deviation } I_{\text{Right}} + \text{Standard deviation } I_{\text{Left}})$$
- **Binary standard deviation method**
Binary standard deviation method depends on P1 value, if it is less than 0.5, the value will be zero. If P1 value is bigger than 0.5, the value is 1
$$\text{Image fused binary standard deviation} = p1 * I_{\text{Right}} + (1-p1) * I_{\text{Left}}$$

- **Real covariance method**
Defined as the square of the standard deviation of a sample or a set of data and was used to analyze the factors that affect the distribution and spread of the data submitted for study. If the P1 value is less than 0.5, the value will be zero.
$$\text{Proposed method P1 covariance} = I_{\text{Right}} / (\text{covariance } I_{\text{Right}} + \text{covariance } I_{\text{Left}})$$
- **binary covariance method**
Binary covariance method depends on P1 value, if it is less than 0.5, the value will be zero. If P1 value is bigger than 0.5, the value is 1
$$\text{Image fused binary standard deviation} = p1 * I_{\text{Right}} + (1-p1) * I_{\text{Left}}$$

3. Results and discussion

The tested images are shown in Figure (1) in the study. Figure 1(a) is the cameraman's image with (256×256) pixel size and 8-bit depth per pixel. Figure 1(b) is a personal image with (473×467) pixel size and 8-bit depth per pixel. Figure 1(c) is the Lena image with (512×512) pixel size and 8-bit depth per pixel.



Figure 1: The images approved in the study (a) Cameraman (b) Personal (c) Lena.

The motion blur method was applied to Figure (1) images with different block sizes (3, 5, 7, 9, and 11). The block was shifted from left to right in the image and from right to left, as shown in Figure (2).

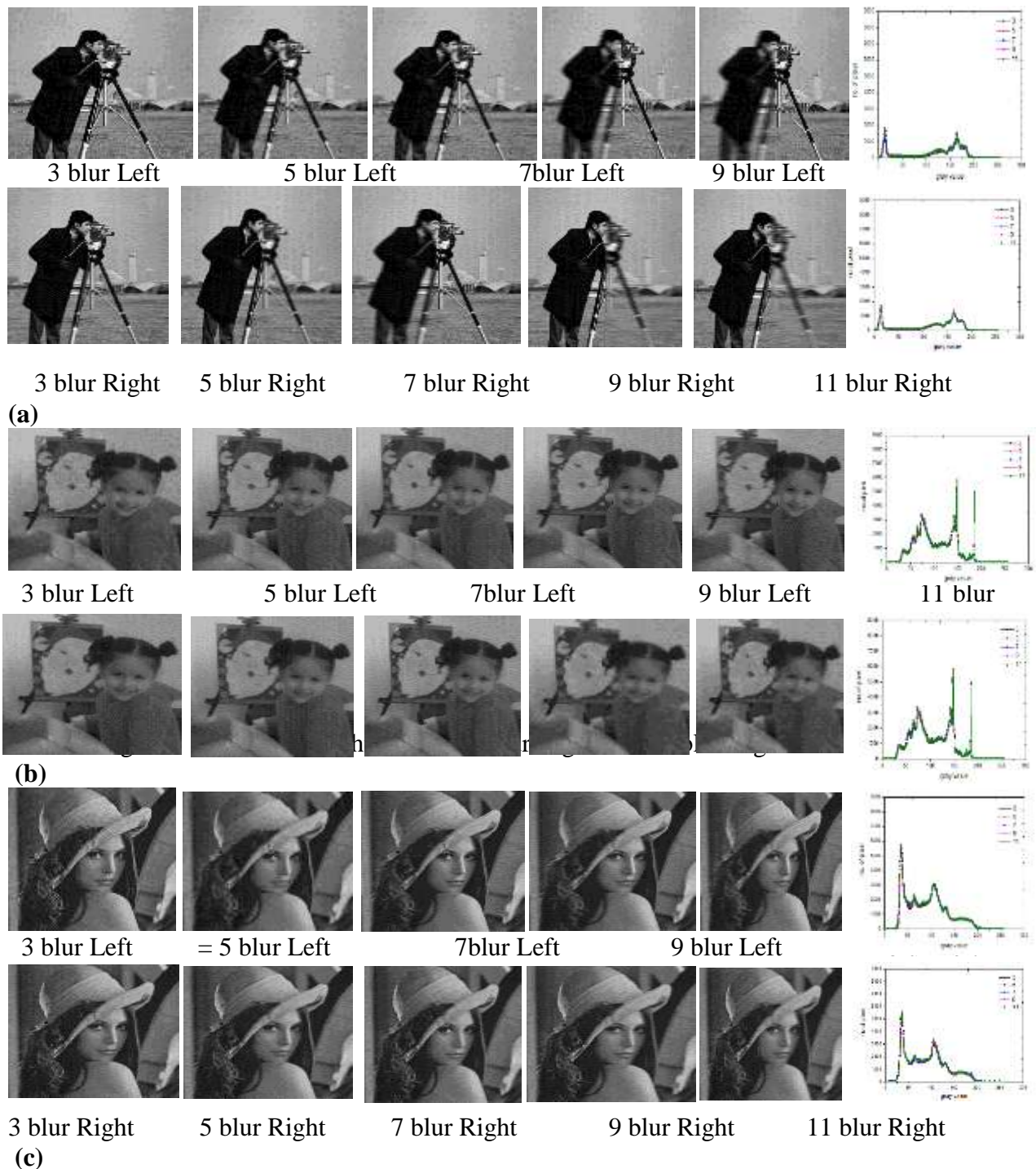


Figure 2: The images resulting from the process of motion blur towards the left and right with their histogram (a) Cameraman (b) Personal images (c) Lena images.

Figure 3 shows Cameraman image fusion with the proposed methods (addition, multiplication, real standard deviation, binary standard deviation, real covariance, and binary covariance) for cameraman images.

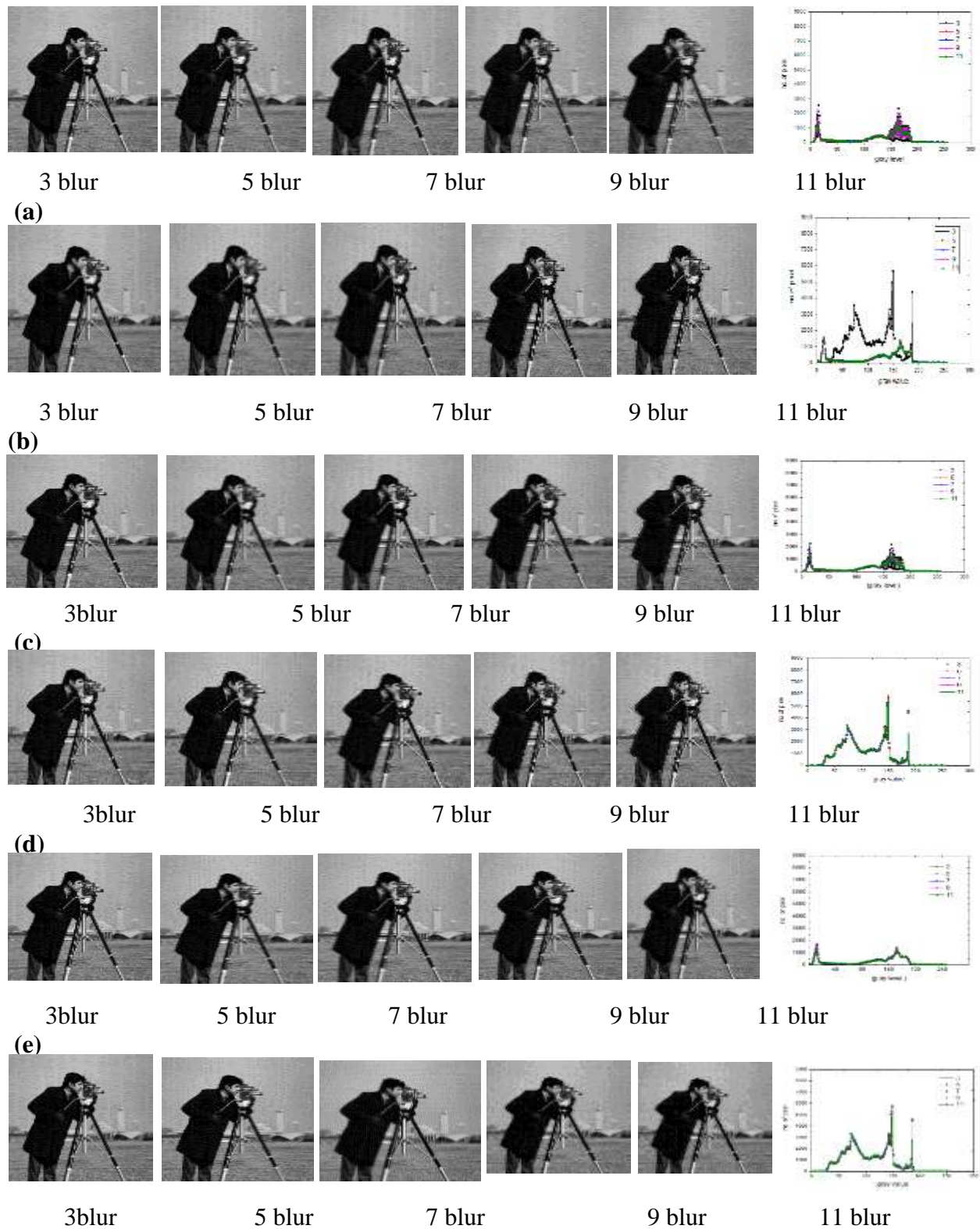


Figure 3: Cameraman fusion image with their histogram using (a) Addition technique, (b) Multiplication technique, (c) Real standard deviation technique, (d) Binary standard deviation technique, (e) Real covariance technique, (f) Binary covariance technique.

Figure 4 shows Personal image fusion with the proposed methods (addition, multiplication, real standard deviation, binary standard deviation, real covariance, and binary covariance) for cameraman images.

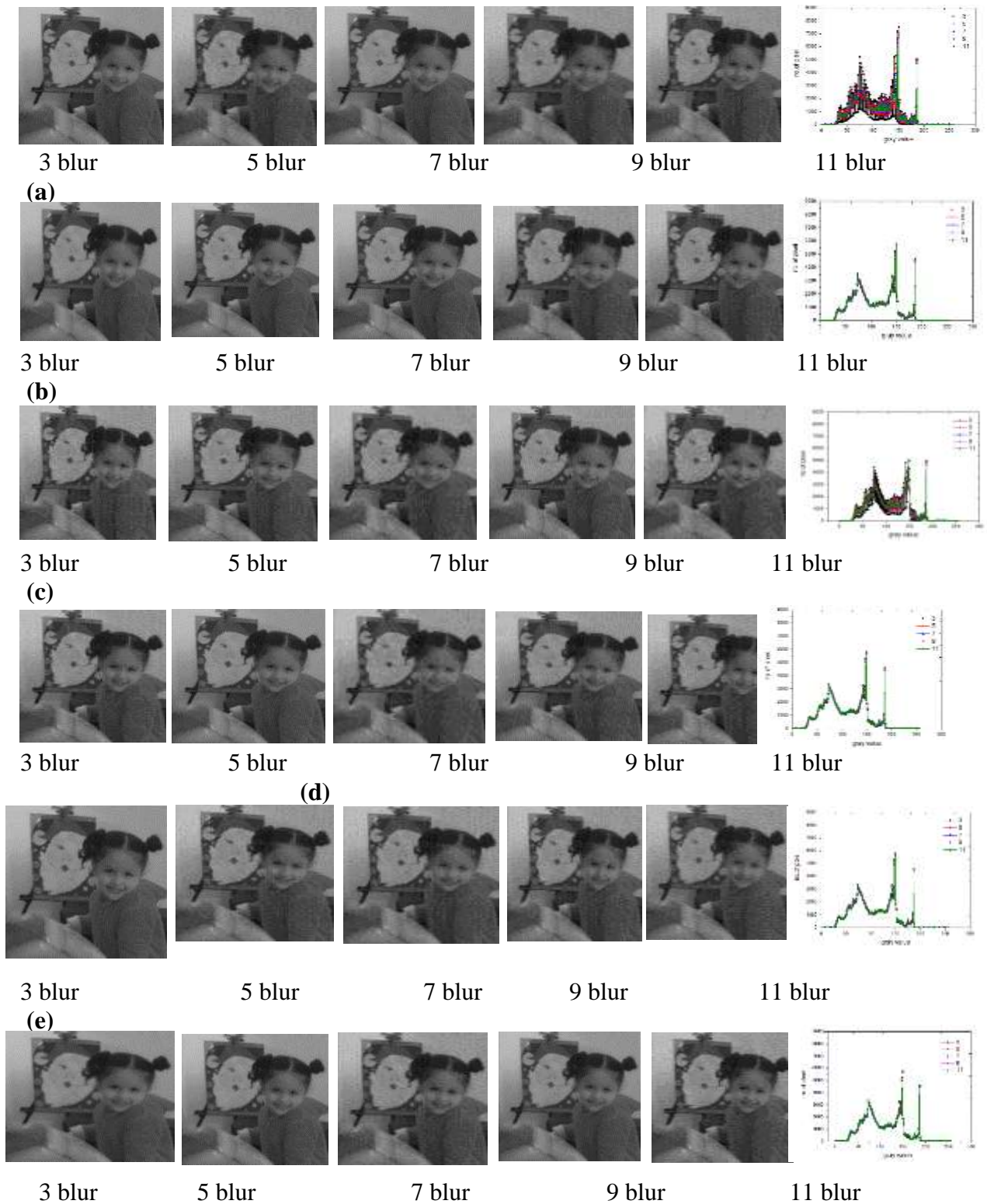


Figure 4: Personal fusion image with their histogram using (a) Addition technique, (b) Multiplication technique, (c) Real standard deviation technique, (d) Binary standard deviation technique, (e) Real covariance technique, (f) Binary covariance technique.

Figure 5 shows Lena's image fusion with the proposed methods (addition, multiplication, real standard deviation, binary standard deviation, real covariance, and binary covariance) for the cameraman image.

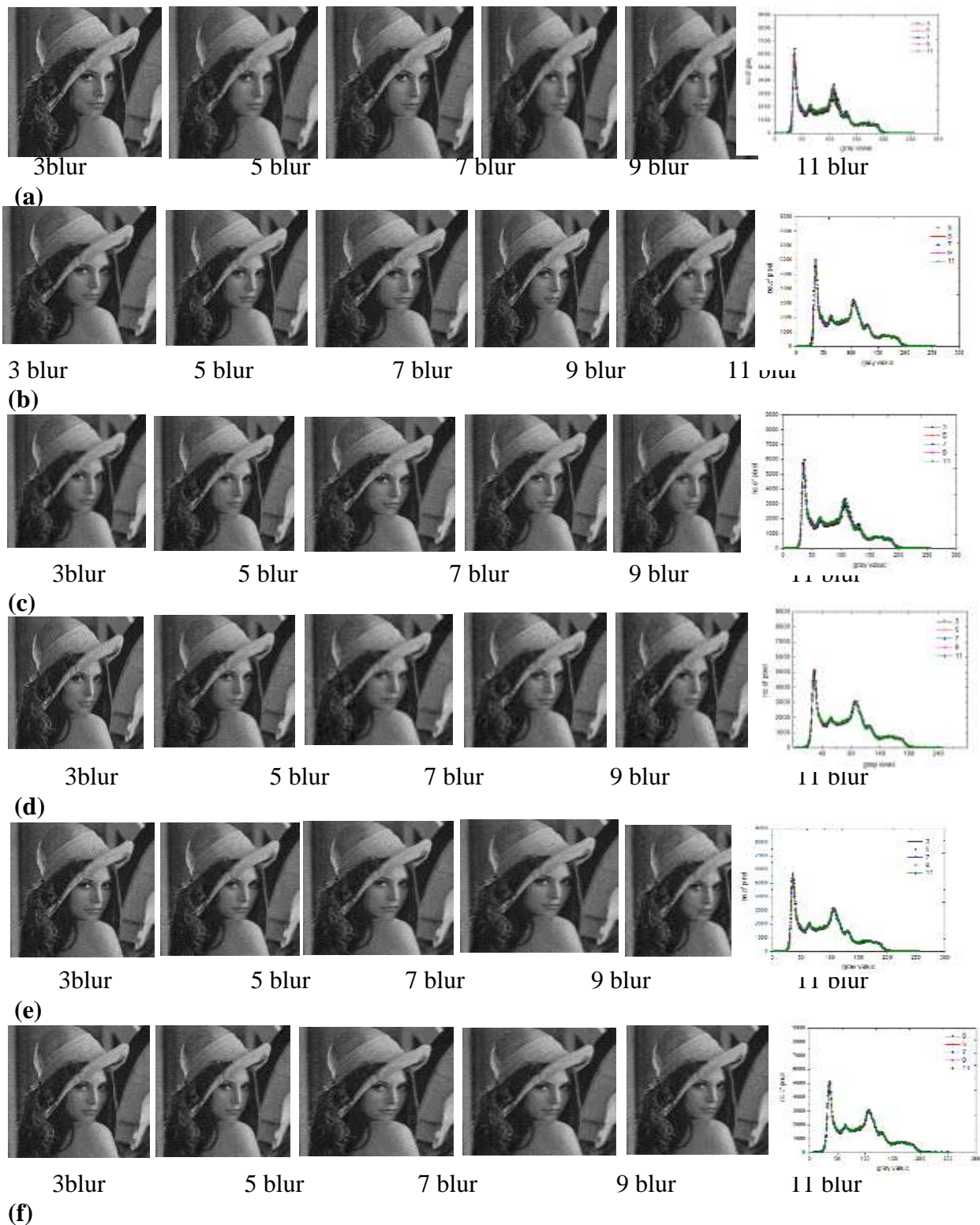


Figure 5: Lena fusion image with their histogram using (a) Addition technique, (b) Multiplication technique, (c) Real standard deviation technique, (d) Binary standard deviation technique, (e) Real covariance technique, (f) Binary covariance technique.

Figure 6 shows the statistical criteria concerning the blur right image (A), blurred left image (B), and fused image (C). Figure 6i is the Mutual Information criteria. Figure 6i (a, c, e) between A and C. While Figure 6i (b, d, f) between B and C. The three images' data in Figure 6i are divided as Lena in (a, b), cameraman in (c, d), and personal in (e, f); this sequence order is the same for the remaining parts in Figure 6. Figure 6ii is the correlation criteria. Figure 6iii is the Normalized cross-correlation criteria. Figure 6iv is the structural similarity index metric criteria. Figure 6v is the norm criteria. Finally, Figure 6, vi structural content criteria.

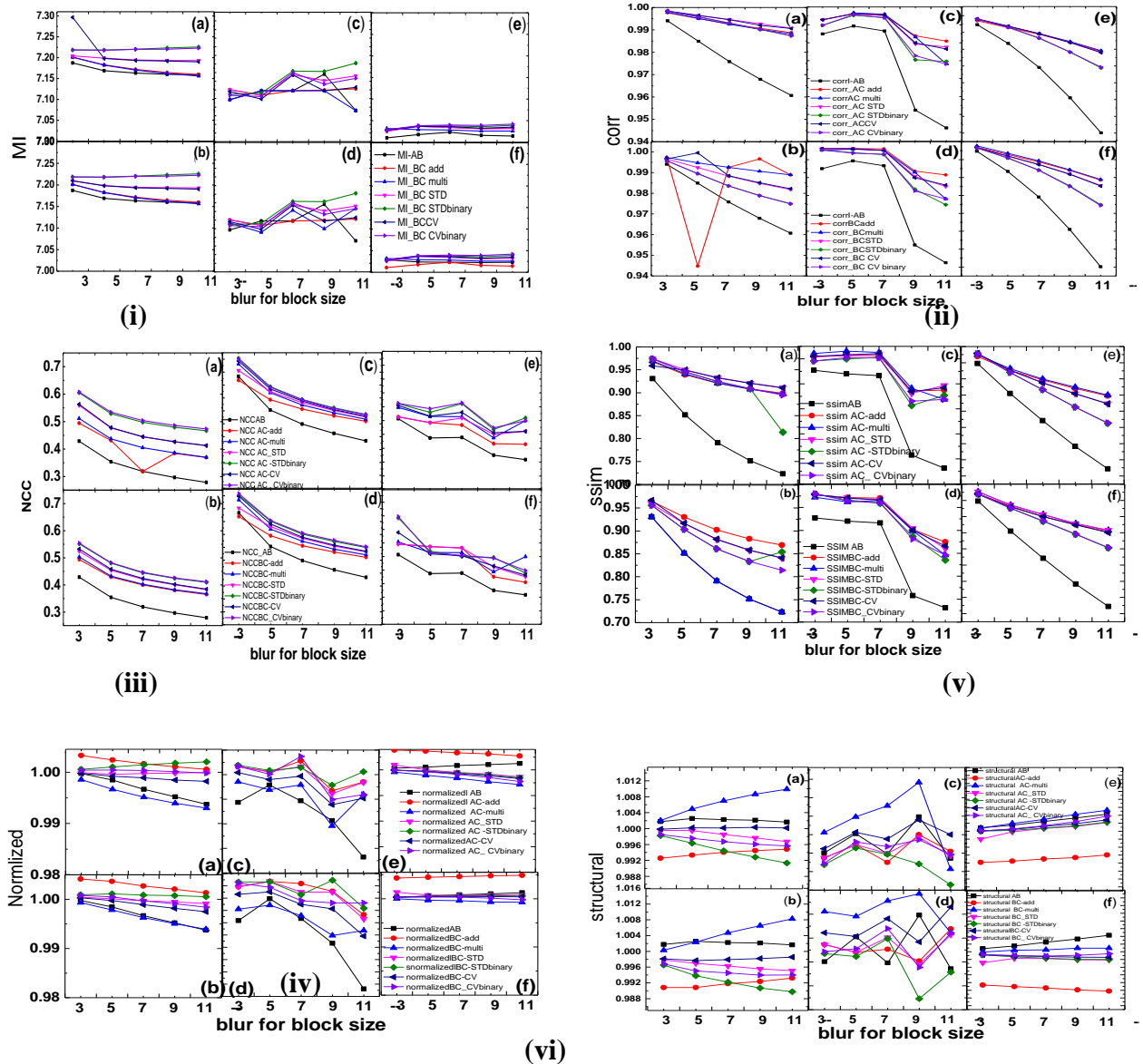


Figure 6: Quality criteria with reference for each blurred image (i) relation between Mutual Information and A, B, and C images (ii) relation between the correlation coefficient and A, B, and C images (iii) relation between normalized cross-correlation and A, B and C images (v) relation between structural similarity index metric and A, B and C images (iv) relation between normalized A, B and C and (vi) structural content A, B, and C images.

Figure 6 shows the cross-correlation criteria, normalized cross-correlation criteria, and structural similarity index metric criteria, clearly showing the blur image's quality behavior. The behavior of the criteria increases with increased blur block size. The higher curve of these methods was the best method. This is because mathematical equations depend on pixel value

or matching between the original and fuse image, while structural content criteria decrease with an increased block size of motion blur for all images. Mutual Information and a random behavior in the cameraman image.

Evaluating the quality of the fused image calculated relied on statistical criteria without reference to a source A and B, as shown in Figures (7) for adopted images (a) Lena, (b) Cameraman, and (c) Personal image. The data explain the relation between A, B, and C criteria.

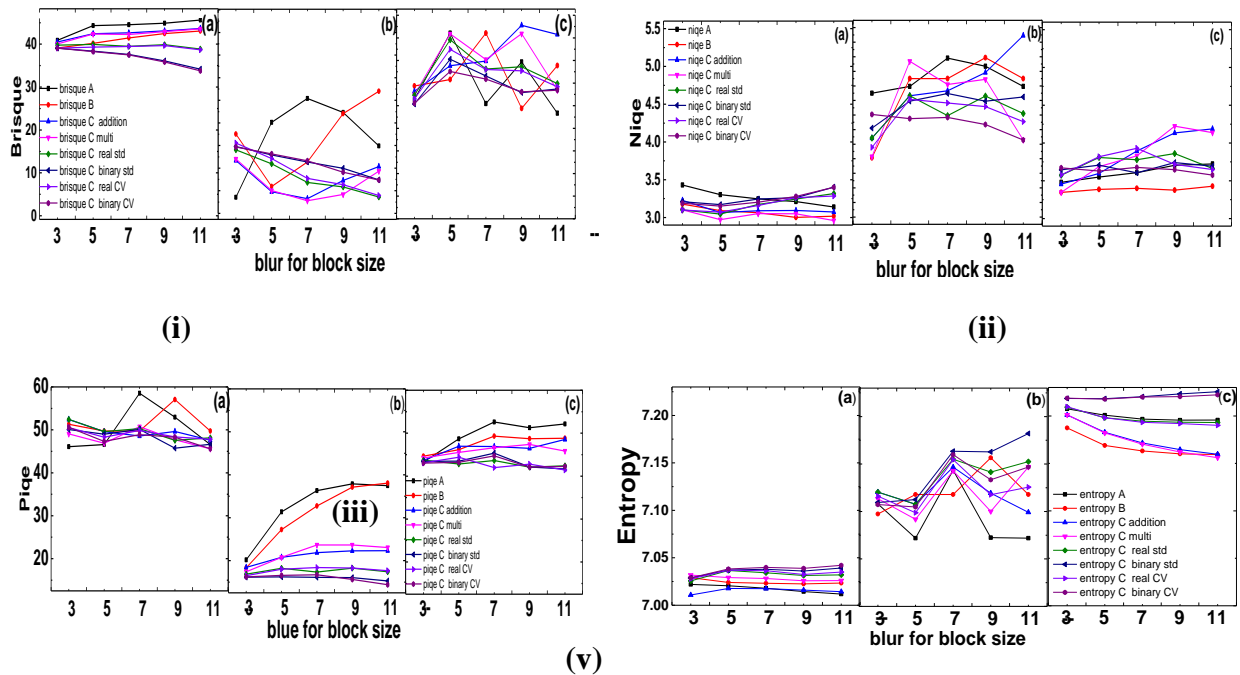


Figure 7: Quality criteria without reference for each blurred image (i) BRISQUE for A, B, and C images (ii) NIQE for A, B, and C images (iii) PIQUE for A, B and C images (v) Entropy for A, B and C images.

Figure 7 shows that the BRISQUE and NIQE behavior of the criterion was constant with increasing block size in Lena's image, the personal image, and randomly in the cameraman's image. PIQUE criteria decrease with the increase of blur block size in the three approved images.

Conclusions

The blurred image was simulated using motion blur type linear homogenous with block size (3, 5, 7, 9, and 11) pixels. The linear direction was from right to left. Therefore, the blurred image was simulated into two halves. The fusion methods (addition, multiplicative, real standard deviation, binary standard deviation, real covariance, and binary covariance) are tested with three gray images. The performance of these methods was evaluated using 10 types of criteria (six with reference and four without reference). The best combination method was binary covariance and binary standard deviation. The cameraman and personal fused image show the same quality, but Lena's image showed different behavior because Lena's image was considered a reference image.

References

- [1] J. Du, W. Li, K. Lu, and B. Xiao, "An overview of multi-modal medical image fusion," *Neurocomputing*, vol. 215, pp. 3-20, 2016.
- [2] H. K. Abbas, A. H. Al-Saleh, H. J. Mohamad, and A. A. Al-Zuky, "New algorithms to enhanced fused images from auto-focus images," *Baghdad Sci. J.*, vol. 10, no. 18, pp. 1, 2021.
- [3] J. Zhang, F. He, Y. Duan, and S. Yang, "AIDEDNet: Anti-interference and detail enhancement dehazing network for real-world scenes," *Frontiers of Computer Science*, vol. 17, no. 2, pp. 172703, 2023.
- [4] A. I. Abas and N. A. Baykan, "Multi-focus image fusion with multi-scale transform optimized by metaheuristic algorithms," *Traitement du Signal*, 2021.
- [5] J. Abbasi Aghamaleki and A. Ghorbani, "Infrared and visible image fusion based on optimal segmenting and contour extraction," *SN Applied Sciences*, vol. 3, pp. 1-14, 2021.
- [6] M. Arif and G. Wang, "Fast curvelet transform through genetic algorithm for multimodal medical image fusion," *Soft Computing*, vol. 24, no. 3, pp. 1815-1836, 2020.
- [7] Y. Li, X. Shen, and H. Chen, "Pyramid Pooling Dense Convolutional Neural Network for Multi-focus Image Fusion," in *2019 IEEE 6th International Conference on Cloud Computing and Intelligence Systems (CCIS)*, 2019: IEEE, pp. 164-168.
- [8] H. K. Abbas, A. H. Al-Saleh, H. J. Mohamad, and A. A. Al-Zuky, "Feature Extraction in Six Blocks to Detect and Recognize English Numbers" *Baghdad Sci. J.*, vol. 62, no. 10, pp. 3790–3803, 2021.
- [9] N. H. Resham, H. K. Abbas, and H. J. Mohamad "Detection and Recognition of Car Plates in Parking Lots at Baghdad University" *Iraqi Journal of Science*, vol. 64, no. 2, pp. 1018–1029, 2023.
- [10] N. H. Resham, H. K. Abbas, H. J. Mohamad, & A. H. Al-Saleh "Noise Reduction, Enhancement and Classification for Sonar Images" *Iraqi Journal of Science*, vol. 62, no. 11, pp. 4439–4452, 2021.
- [11] S. C. Kulkarni and P. P. Rege, "Pixel level fusion techniques for SAR and optical images: A review," *Information Fusion*, vol. 59, pp. 13-29, 2020.
- [12] B. O. Adame, A. O. Salau, B. C. Subbanna, T. Tirupal, and S. F. Sultana, "Multimodal medical image fusion based on intuitionistic fuzzy sets," in *2020 IEEE International Women in Engineering (WIE) Conference on Electrical and Computer Engineering (WIECON-ECE)*, 2020: IEEE, pp. 131-134.
- [13] Q. Xin, S. Hu, S. Liu, L. Zhao, and Y.-D. Zhang, "An attention-based wavelet convolution neural network for epilepsy EEG classification," *IEEE Transactions on Neural Systems and Rehabilitation Engineering*, vol. 30, pp. 957-966, 2022.
- [14] Y. Xiao, Z. Guo, P. Veelaert, and W. Philips, "DMDN: Degradation model-based deep network for multi-focus image fusion," *Signal Processing: Image Communication*, vol. 101, pp. 116554, 2022.
- [15] W. Zhou et al., "Improved estimation of motion blur parameters for restoration from a single image," *Plos one*, vol. 15, no. 9, pp. e0238259, 2020.
- [16] M. H. Nadimi-Shahraki, S. Taghian, and S. Mirjalili, "An improved grey wolf optimizer for solving engineering problems," *Expert Systems with Applications*, vol. 166, pp. 113917, 2021.
- [17] G. Zhang and T. Zheng, "Estimation method of blurred parameters in moving blurred image," in *Journal of Physics: Conference Series*, 2020, vol. 1616, no. 1, pp. 012096.
- [18] T. Askari Javaran and H. Hassanpour, "Using a Blur Metric to Estimate Linear Motion Blur Parameters," *Computational and Mathematical Methods in Medicine*, vol. 2021, pp. 1-8, 2021.
- [19] K. A. Dar and S. Mittal, "A Dynamic Fuzzy Histogram Equalization for High Dynamic Range Images by Using Multi-Scale Retinex Algorithm," in *Proceedings of the International Conference on Innovative Computing & Communications (ICICC)*, 2020.
- [20] H. K. Abbas, A. H. Al-Saleh, and A. A. Al-Zuky, "Optical Images Fusion Based on Linear Interpolation Methods," *Iraqi Journal of Science*, vol. 60, no. 4, pp. 924-936, 2019.
- [21] W. Lu et al., "Blind Surveillance Image Quality Assessment via Deep Neural Network Combined with the Visual Saliency," in *Artificial Intelligence: Second CAAI International Conference*,

- CICAI 2022, Beijing, China, August 27–28, 2022, Revised Selected Papers, Part II, 2023: Springer, pp. 136-146.*
- [22] G.-H. Gwon, J. H. Lee, I.-H. Kim, and H.-J. Jung, "CNN-based Image Quality Classification Considering Quality Degradation in Bridge Inspection using an Unmanned Aerial Vehicle," *IEEE Access*, 2023.
- [23] M. A. Aljanabi, Z. M. Hussain, N. A. A. Shnain, and S. F. Lu, "Design of a hybrid measure for image similarity: a statistical, algebraic, and information-theoretic approach," *European Journal of Remote Sensing*, vol. 52, no. sup4, pp. 2-15, 2019.
- [24] X. Lei, Y. Xia, A. Wang, X. Jian, H. Zhong, and L. Sun, "Mutual information based anomaly detection of monitoring data with attention mechanism and residual learning," *Mechanical Systems and Signal Processing*, vol. 182, pp. 109607, 2023.
- [25] Q. Sang, Y. Yang, L. Liu, X. Song, and X. Wu, "Image quality assessment based on quaternion singular value decomposition," *IEEE Access*, vol. 8, pp. 75925-75935, 2020.
- [26] L. Wu and L. Zhao, "ISAR Image Registration Based on Normalized Correlation Coefficient," in *2023 IEEE 3rd International Conference on Power, Electronics and Computer Applications (ICPECA)*, 2023: IEEE, pp. 354-359.
- [27] L. Wu, X. Zhang, H. Chen, D. Wang, and J. Deng, "VP-NIQE: An opinion-unaware visual perception natural image quality evaluator," *Neurocomputing*, vol. 463, pp. 17-28, 2021.
- [28] S. A. Golestaneh, S. Dadsetan, and K. M. Kitani, "No-reference image quality assessment via transformers, relative ranking, and self-consistency," in *Proceedings of the IEEE/CVF Winter Conference on Applications of Computer Vision*, 2022, pp. 1220-1230.
- [29] S. K. Panguluri and L. Mohan, "Discrete wavelet transform based image fusion using unsharp masking," *Periodica Polytechnica Electrical Engineering and Computer Science*, vol. 64, no. 2, pp. 211-220, 2020.